Optical microscopy of Au nanoparticle arrays fabricated by Nanosphere lithography (NSL) under swift heavy ion beam irradiation

E. A. Dawi* [a, b] and F.H.P.M. Habraken [b]

Abstract — A simple, yet effective technique known as nanosphere lithography (NSL) is used to fabricate close-packed hexagonal arrays of Au nanoprisms.

Colloidal patterning employs two variants of regular masks formed by self-assembly of respectively 700- to 1400nm diameter silica colloids form a hexagonal close-packed single layer on a Si/SiO2 surface. First, unmod ified silica deposition mask with 700±10 nm colloidal diameter is used to fabricate single layer periodic particle domains of Au nanoprisms by thermal evaporation of Au through the colloidal mask hole. After annealing to 900 °C for an hour, most of the Au nanoprisms are transformed into rounded nanoparticles with 80-100 nm diameter.

In the second variant, an in-plane expansion of the colloids in the colloidal deposition mask with 1400±20 nm colloidal diameter is induced by irradiation with 30 MeV Si+5 and 6 MeV Ag+3 ions at 90 K and normal incidence. The latter treatment allows to systematically vary the size and morphology of Au nanoparticles to reach a deformable range of 50-65 nm diameter for the nanoparticles. After removal of the mask, sputter deposition of a second oxide layer and annealing, the silica films containing the embedded particles are post-irradiated with 50 MeV Ag+7 ions at 300 K and at normal incidence. Dark-field light-scattering experiments performed on the fabricated Au nanoparticles with 50-65 nm diameter before and after irradiation revealed a true color-change within the regular scattering pattern indicating that the surface plasmon resonance band has shifted as a result of the ion-shaping effects.

Index Terms— Au nanoparticles, electrostatic coupling, nano-sphere lithography, optical microscopy, ion beam, silica matrix, close-packed hexagonal arrays

1 INTRODUCTION

Conventional methods such as photolithography and focused ion beam lithography are routinely used to create nanostructures with controlled size, shape, and well optimized spacing length [1], [2], [3], [4]. Such tools are generally time-consuming and their costs are considerably higher. Soft lithography techniques, although they present many advantages, do require the production of a single mask (which will be used several times) by conventional lithographic techniques. A faster method to fabricate particle arrays by using two-dimensional self-assembled colloidal silica particles as a deposition mask has been reported many times in literature [5], [6], [7], [8], [9], [10]. Such method is called nanosphere lithography (NSL) and to our knowledge it was explored during the early eighties of the last century by Fischer and Zingsheim [11] and, subsequently, Deckman and Dunsmuir [12], [13]. Within this method, the flat substrate is coated with a suspension containing monodisperse spherical colloids (e.g., polystyrene) after a chemical treatment to enhance its hydrophilic character. Upon drying, a hexagonal-close-packed (HCP) monolayer or bilayer, called a colloidal crystal mask (CCM), is self-assembled. This mask is then used to selectively pattern the substrate, thanks to the deposition of the material of interest through the interstices of the ordered colloids. Self-assembly however, has its own problem of regularity and reproducibility. Indeed, control of the density and shape of the nanostructures is difficult to achieve, which is rather complex especially in case of magnetic data storage.

The simplicity of NSL originates from the easy removal of the colloidal mask providing arrays of patterned particles left over on the substrate. An average particle diameter not below 100 nm is expected to form. Such particles can be used in a wide range of applications. For example, arrays of metallic nanoparticles (NPs) intensify the optical fields providing the possibility for electro-chemical and biomedical detection [14], [15].

A wealth of different studies involving the NSL has already been reported. M. Winzer and co-workers fabricated arrays of nanometer scale Au and Co particles [16]. A detailed investigation of NSL in fabrication of new structural NP systems has

- *E.A. Dawi, corresponding author: Ajman University, Department of Basic Science and Mathematics, P.O.Box 346, Ajman, UAE.*
- *F.H.P.M. Habraken, Debye institute for nanomaterials, Utrecht University, Domplein 29, 3512JE, Utrecht, the Netherlands.*

been carried out by P. Van Duyne et al. [17]. X. Huang et. al. [18] and co-workers have fabricated large-area hexagonal arrays of metallic nanodiscs using an NSL template combined with a two-step lift-off process. Periodic particle arrays using single and double-layer masks polymer have been demonstrated by John C. Hulteen et. al. [19]. In a process combining NSL and reactive ion etching (RIE), C. X. Cong [20] and co-workers have fabricated ordered graphene nano-disk arrays. Furthermore, Traci R. Jensen et. al. [21] fabricated Ag nanoparticles that displayed localized surface plasmon resonances, LSPRs, tunable throughout the visible, near-infrared, and mid-infrared regions of the electromagnetic spectrum using NSL.

Although NSL has been further developed, the existence of single vacancies, dislocations, grain boundaries and double layer periodic crystal arrays represents some of the major disadvantages within the technique. However, the defect-free regions are large enough for microscopic imaging.

Introducing the ion beam irradiation at ~MeV kinetic energy as a hammering tool to tune the size and shape of the silica colloidal particles has recently been described in a number of studies [22], [23], [24], [25]. D. Vossen et al. [26], [27] show that irradiation with 4 MeV Xe^{+4} ions of a spherical silica colloidal mask induces the in-plane expansion of colloidal silica particles perpendicular to the ion beam direction. Consequently, a controllable adjustment of the colloidal mask hole size is established. The latter allows the fabrication of arrays of metallic NPs of different size by evaporating the desired type of metal through the holes of the colloidal mask.

Collective excitations of conduction electrons in metal NPs known as surface plasmons (SPs) determine to a large extent the optical response of the material structure. The resonance frequency at which the free electrons oscillate in response to the alternating electric field of incident electromagnetic radiation determines the colour of the NPs , at least when this falls in the visible range. As the size or shape of the NP changes, the observed color of the NP also changes. The ion beam shaping technique is becoming, in this respect, a powerful tool to manipulate matter at the nanometer scale. It allows us to transform spherical dielectric particles into oblate nanostructures, i.e., with their elongation normal to the beam direction, and metal NPs confined within a dielectric matrix into prolate nanorods and nanowires with their elongation along the beam direction. A detailed investigation of the irradiation-induced deformation has been carried out by Polman's group for NPs with a core-shell configuration, namely, a Au-core/silica-shell ($Au@SiO_2$) system [28], [29], [30). Systematic investigation of the role played by metallic NP size and density within the elongation mechanism has been carried by the authors and co-workers [31], [32], [33], [34]. A theoretical interpretation based on the thermal-spike model, has been proposed by Awazu et al. [35] The thermodynamic properties of ion-shaped metallic NPs have been studied by Ridgway's group with synchrotron techniques. [36], [37], [38], [39]. Rational description of the ion-beam shaping mechanism have been carried out by Rizza et al. [40]. Dufour et al.have implemented the thermal-spike model in three dimensions and for anisotropic and composite media. [41]

Although the mechanism governing the ion induced shaping of metallic NPs is still not well known, the NP size has experimentally been found to be a crucial parameter for the shaping characteristics. Few theoretical studies have been attempted to understand the NPs deformation on basis of the thermal spike model, where the deformation is attributed to melting of the metal NP and/or of the surrounding silica matrix [42], [43]. Nevertheless, further investigation on the role of the initial configuration of the NPs and the irradiation parameters is required.

This paper has a two-fold objective: (1). Report the fabrication of 2-dimensional arrays of Au NPs with size ideally in the range of 50-60 nm diameter by using NSL method and (2) Report the investigations of the ion-shaping effects within the fabricated NPs by using dark-field light scattering optical microscope, making use of the phenomenon that surface plasmon resonance of such spherical NPs can be red-shifted by changing their size aspect ratio.

2 METHOD

The basic scenario of NSL includes the formation of a single layer of silica colloids self-organized onto the substrate. Colloidal silica particles have the advantage of being single crystals with typically atomic scale surface roughness. However, it is difficult to arrange these particles into desired configuration due to the fact that the colloidal particles are distributed randomly in the colloidal solution. The successful colloidal deposition method requires a migration of silica colloids on the substrate, seeking their minimum energy configuration. To achieve this, an ultra-clean sample surface is of great importance. In the work presented, the 1x1 cm^2 thermally oxidized Si substrates are cleaned by distilled water and immersed afterwards in a beaker containing 80 ml of ethanol with 99.9% purity for 30 minutes. The substrates are rinsed by highly purified methanol and distilled water before finally being dried by a nitrogen flow. Throughout our experimental procedures, two colloidal deposition schemes have been

found to provide the best results in the formation of a mono-layer of self-organised colloidal silica particles. The first scheme comprises the self-assembly of a colloidal mask by spin-coating (3250 rpm) of 15 µL colloidal solution (700 nm colloidal diameter, 0.9 % volume) dropcasted on the substrate surface. In the second scheme, a technique is developed to obtain single layer domains of several tens of square micrometers area after evaporation to dryness of 12 µL colloidal solution (1.4 µm diameter, 0.7 % volume) being dropcasted on the substrate surface. In both deposition schemes, the Si/SiO2 substrates are given positive surface charge in order to electrostatically couple the negatively charged monodisperse silica colloids to the surface. To achieve the charging, the substrates are immersed in a mixture of aminopropyl triethoxy/methoxysilane (APTEMS) and ethanol in a ratio of 1:6 (by volume). The substrates are left to react with the solution for half an hour before they are rinsed by methanol and distilled water and finally dried by nitrogen flow. Upon solvent evaporation, the colloidal silica film re-crystallizes forming single and bi-layer arrangements on the surface of the substrate. The mean size and the polydispersity of the silica colloids are determined from scanning electron microscope (SEM) experiments performed with applied voltage between 1-20 keV on several hundreds of silica particles. Average diameter of the two kinds of the patterned silica particles is about 700 ± 10 nm and 1400 ± 20 nm (centre-to-centre distance), respectively. The perpendicular bisector, a, of the hole created by the three-fold interstices represents the colloidal mask hole size. It is found from geometrical calculations [17] that the relationships between the mask hole size a, the diameter of the silica particle D, and the interparticle spacing dip, can be given by the equations:

$$a = 3/2\ [(\sqrt{3}-1)-(1/\sqrt{3})]\ D$$

Where;

$$D = (3d_{ip})^{1/2}$$

d_{ip} is the interparticle distance.

Thus, modifying in a controlled way one of these parameters represents a way to control the mask hole size and consequently the size of the fabricated metal NPs. General overview of the experimental procedures followed in the second deposition scheme is shown in figure 1.

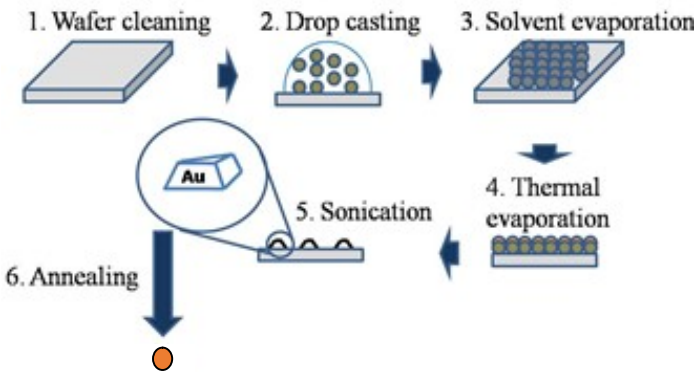

Fig 1 Schematic illustration of the experimental procedures followed in fabrication of arrays of Au NPs by using the 1.4 µm diameter silica colloids as deposition mask.

Preliminary irradiations with 30 MeV Si^{+5} and 6 MeV Ag^{+3} ions have been performed on the Si/SiO_2 substrates containing only the silica particles of 1.4 µm colloidal diameter. As an impact of these preliminary irradiations, the originally spherical silica colloidal particles undergo anisotropic deformation such that the particle expands in a direction perpendicular to the ion beam direction, and contracts parallel to it. Consequently, the colloidal mask hole size could be optimized. Irradiations are performed at 90 K applying normal incidence geometry for fluences ranging between 10^{13} and 10^{14} ions/cm^2. The ion beams are electrostatically scanned for homogenous irradiation over the entire sample area. Samples are mounted on a copper block using conductive paste. During irradiation liquid nitrogen is used to cool the samples. The projected range of the ion energies is obtained from SRIM code [44] and found to be about 10.2 and 2.8 µm for 30 MeV Si^{+5} and 6 MeV Ag^{+3} ions, respectively. These ranges are far beyond the thickness of the silica deposition mask. After colloidal patterning and irradiation, thermal evaporation was subsequently used to deposit gold through the colloidal mask layer to generate ordered arrays of Au nanoprisms in a hexagonally close-packed arrangement. The pressure during the evaporation process was $1.5x10^{-6}$ mbar. In the evaporation chamber, samples are mounted on a copper holder and placed at a distance of 10 cm above a filament boat containing the evaporant. The vapor path is always perpendicular to the sample surface. The amount of the Au evaporated through the holes consequently determines the thickness of the Au nanoprisms. Figure 2 show

SEM images of arrays of Au nanoprisms fabricated by evaporation of different amount of Au powder through a mask hole size of 350-400 nm. The volume of the evaporated Au powder is measured by a digital mass balance. For the different Au volumes of 5, 15, 25 and 40 μg, the corresponding thickness of the fabricated Au nanoprism is deduced from atomic force microscopy experiments (AFM) by measuring the particle height and found to be about 18 (a), 28 (b), 45 (c) and 60 (d) nm, respectively. Under these experimental conditions the diameter of the fabricated spherical NPs is predicted to be approximately 100, 140, 160 and 180 nm, respectively.

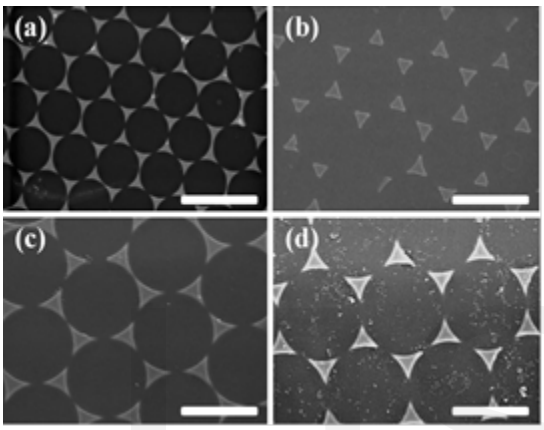

Fig. 2 Overview of hexagonal close-packed arrays of Au nanoprisms fabricated by thermal evaporation of different volumes of Au powder through silica colloidal crystal mask (1.4 μm colloidal diameter). The scale bar is 2 μm in image (a), 1.5 μm in image (b) and 1 μm in (c) and (d), respectively.

In this work, we will only use an amount of 40 μg Au powder to fabricate our Au nanoprisms and further tune the hole size by tuning the irradiation energy specified above. The corresponding thickness of the fabricated nanoprisms as we mentioned earlier is about 60 nm. After metal evaporation, subsequent removal of the mask (lift-off) by sonication of the samples in a basin of water at high frequency is applied to remove the colloidal mask. During sonication, the samples are immersed into highly-purified ethanol in a glass beaker to avoid contamination. After sonication, the samples with the replicated Au nanoprisms are annealed at 900 °C for an hour to crystallize the sample or/and induce a crystallographic phase change. SEM images of the surface of the samples after annealing show that most of the metallic nanoprisms are transformed into rounded NPs. A SiO_2 film with a thickness of 150 nm is reactively sputtered encapsulating the fabricated Au NPs in a 350 nm silica film and the sample is once again annealed at 900 °C for 15 minutes. Samples are subsequently irradiated with 50 MeV Ag+7 ions to investigate the irradiation induced-shaping effects on the fabricated Au NPs. The projected range of silver ions with this energy is deduced from SRIM code and found to be about 9.7 μm. Hence, the irradiation is only used to deposit energy into the SiO_2-Au layers. The post irradiation is performed at room temperature (300 K) applying normal incidence for fluences in the order of 10^{14} to few 10^{15} ions/cm^2.

3 Results and Discussion

For the sake of clarity the presentation of the experimental results has been organized in two subsections. In the first one, we present the results of the fabrication of two-dimensional arrays of Au NPs by using the two deposition schemes of the silica colloids. In the second subsection, the influence of the ion-shaping process on the optical characteristics of the fabricated Au NPs is described.

3.1 Fabrication of hexagonal arrays of Au NPs using NSL

3.1(I) Fabrication of Au NPs by using the unmodified mask of 700 nm diameter

Figures 3(a-b) show SEM images of hexagonal close-packed arrays of Au NPs fabricated by using 700 nm silica colloids as deposition mask, after removal of the colloids, before (a) and after (b) annealing to 900 °C for 1 hour, respectively.

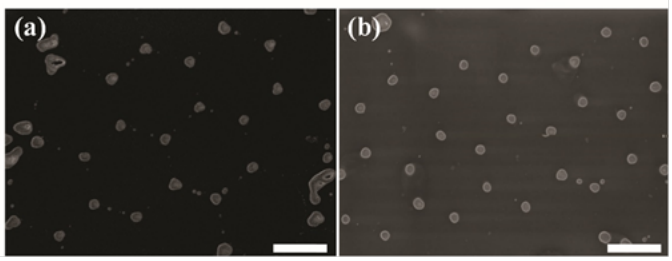

Fig. 3 Arrays of hexagonal close-packed Au nanoprisms immobilized on Si/SiO_2 substrate fabricated by using 700 nm silica colloids as deposition mask before and after annealing at 900 °C for 1 hour, (a) and (b), respectively. The fabricated Au nanoprisms are transformed into rounded NPs of about 80-100 nm diameter. Both images are taken after removal of the

colloidal mask. The length of the scale bar is 500 nm.

Unfortunately, the deposition scheme by using the 700 nm silica colloids appears to suffer from a number of limitations, such as lack of control over the packing morphology of the fabricated Au NPs. In this sense, we found that most of the Au nanoprisms obtained deviated from their predicted quasi triangular shape, presumably due to a slight annealing of the colloidal mask as a result of high evaporation temperature. An example is shown in figure 3(a) which presents a randomly selected region of the samples surface after removal of the colloidal mask. After annealing at 900 °C for an hour, figure 3(b) shows an array of randomly shaped Au NPs including spherical particles with a diameter in the range of 80-100 nm. It should be remarked that following equation 1, the predicted NP size is about 120 nm diameter.

3.1(II) Fabrication of Au NPs by using 1.4 μm silica colloidal mask irradiated with 30 MeV Si^{+5} ions

The SEM image in figure 4(a) shows a region of a colloidal monolayer formed by self-assembly of 1.4 μm silica colloids on the surface of Si/SiO_2 substrate before irradiation with 30 MeV Si^{+5} ions. The colloidal mask hole size is deduced to amount to about 350-400 nm. After irradiation with 30 MeV Si^{+5} ions to a fluence of $6.3x10^{13}$ ions/cm^2, the mask hole size is reduced to ~270 nm as a result of the in-plane expansion of the silica colloids perpendicular to the ion beam direction. The topography of the sample surface after irradiation to this fluence is represented by figure 4(b). At this point, the sample surface is imaged once more after evaporation of 40 μg of Au through the mask and removal of the colloidal mask by sonication [see figure 4(c)]. Under irradiation to a fluence of $2.5x10^{14}$ ions/cm^2, the colloidal mask hole size is further reduced to 200 nm. The surface image corresponding to the irradiation with this fluence is shown in figure 4(d). Figure 4(e) shows the sample surface after Au evaporation and removal of the colloidal mask represented by figure 4(d). After irradiation to a fluence higher than $2.5x10^{14}$ ions/cm^2, it was difficult to completely remove the colloidal mask from the sample surface. It may very well be that the energy deposited by the fast Si ions (3.2 keV/nm in silica) leads to strong contact between the mask and the substrate as a result of the significant local heating even though the samples are cooled during irradiation by using liquid nitrogen. The presence of the non-removable mask provides larger surface roughening which makes it difficult to embed the metallic NPs by successive sputter deposition of a second silica layer. Therefore, for further tuning of the mask hole size and easier removal of the mask, irradiation conditions must be optimized.

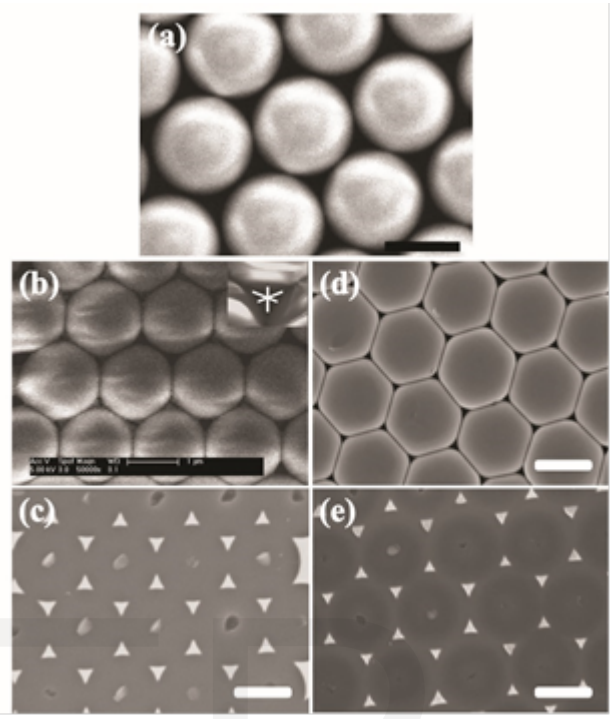

Fig. 4 The colloidal silica deposition mask of 1.4 μm before irradiation with 30 MeV Si^{+3} ions (a) and with irradiation to $6.3x10^{13}$ ions/cm^2 before and after removal of the mask, (b) and (c), respectively and with irradiation to $2.5x10^{14}$ ions/cm^2 before and after removal of the colloidal mask, (d) and (e), respectively. Scale bar in all images is 1 μm.

3.1(III) Fabrication of Au NPs by using 1.4 μm silica colloidal crystal mask irradiated with 6 MeV Ag^{+3} ions

The colloidal silica mask of 1.4 μm diameter has been irradiated with 6 MeV Ag^{+3} ions as an alternative ion energy, at 90 K and normal incidence for fluences in the order of 10^{14}-10^{15} ions/cm^2. With this irradiation energy, we aim to reproduce the similar results reported in references [26] and [27] for irradiation of 1.4 μm silica colloidal mask with 4 MeV Xe^{+4} ions. In this respect, D. Vossen et al. [26] shows that the colloidal mask hole size decreases drastically with further increase of the irradiation fluence. By controling the colloidal mask

hole size this way, it was possible to fabricate Au NPs as small as 20 nm diameter. In fact the electronic stopping of the 6 MeV Ag^{+3} ion energy (2 keV/nm in silica) is not too far from that for 4 MeV Xe^{+4} ions (1.5 keV/nm). In addition, the removal of the colloidal mask by sonication appears much easier even after irradiation to higher fluences. In figure 5, the colloidal mask hole size of a two-dimensional hexagonal lattice of close-packed 1.4 µm diameter silica particles on a Si/SiO_2 substrate is plotted as function of the ion fluence for irradiation with 6 MeV Ag^{+3} ions. A linearly varying ion fluence ranging from zero to $1x10^{15}$ ions/cm^2 across the sample area was thus established. As clearly shown in figure 5, the colloidal mask hole size gradually decreased with increasing the Ag ion fluence until the holes are completely closed. Hole sizes were determined at least three or four rows of particles away from the edges of the domain and an average over six holes was taken.

In view of the experimental results, we found that under irradiation to fluence of $6.0x10^{14}$ ions/cm^2, the fabricated NP size is in the range of 50-80 nm diameter (figure 6). However, non-spherical particles are also produced. This is mainly attributed to the polydispersity in colloid size and colloidal dislocations. To summarize, in this subsection it is shown that we were able to fabricate periodic particle arrays of Au NPs by using two variants of self-assembled colloidal crystal deposition masks. We were able to modify the size and shape of the fabricated Au NPs by adjustment of the deposition mask and alternatively, by optimization of the different irradiation parameters. With regard to the last point, we were able to qualitatively reproduce the results reported in references [22] and [23] for the mask hole size as function of fluence of the 4 MeV Xe^{+4} ion irradiation. On the other hand, the optimization of the precision of size and shape of the fabricated NPs remains a challenging task. Concluding we have shown to be able to fabricate ordered arrays of Au NPs with diameter in the range between 50-100 nm.

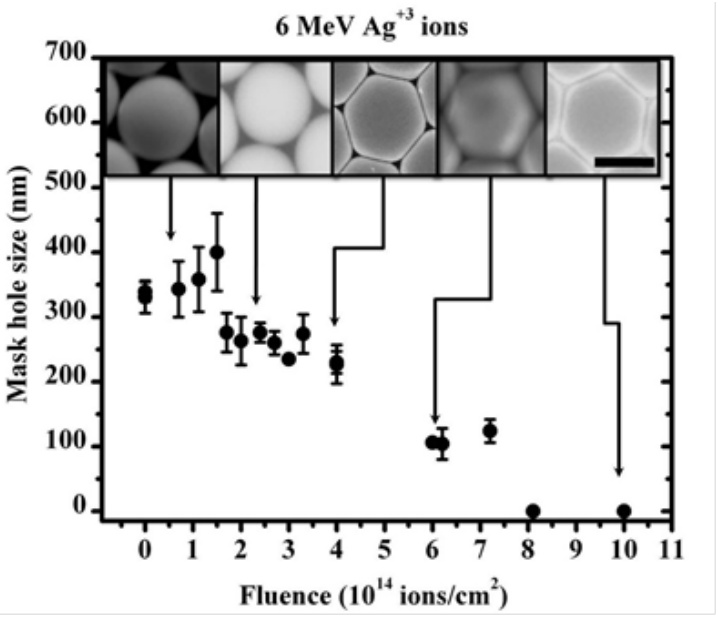

Fig. 5 The measured mask hole size as function of ion fluence for 1.4 µm silica colloidal mask irradiated with 6 MeV Ag^{+3} ions at 90 K and normal incidence. Corresponding images are given in the inset. For all images the same scale bar of 1 µm applies.

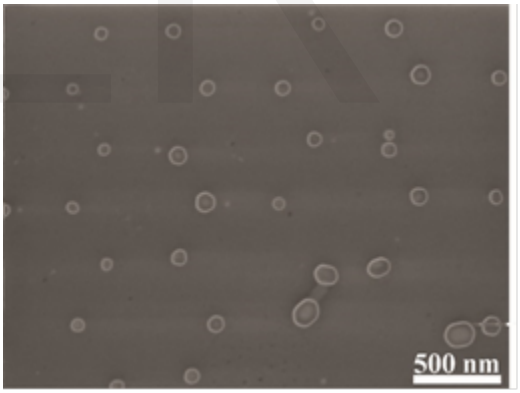

Figure 6 Scanning electron microscopy (SEM) image of arrays of Au NPs with diameter in the range of 50-80 nm fabricated after irradiating the silica colloidal mask with 6 MeV Ag^{+3} ions to a fluence of $6.0x10^{14}$ ions/cm^2.

3.2 Investigations of the ion-shaping effects of ordered arrays of Au NPs by optical microscopy

In this subsection, we investigate the shape change induced by irradiation with 50 MeV Ag^{+7} ions on randomly selected regions containing hexagonal arrays of the fabricated Au NPs. At this stage, irradiations were made at 45° with respect to the sample surface normal. The ion-shaping effects have been investigated by imaging the hexagonal scattering patterns of Au NPs before and after irradiation using dark-field optical microscopy. In this technique the Au NPs are illuminated by white light at a large angle (relative to the normal), and the scattered light is collected at a small angle. By coupling a dark-field microscope to an imaging monochromator and charge coupled device (CCD) camera, NPs in the substrate are photographed obtaining a true color image. We will discuss the shaping effects, first on the larger Au NPs of 80-100 nm diameter fabricated by using the unmodified colloidal mask of 700 nm diameter, and second on the NP size range of 50-80 nm diameter fabricated by modification of the 1.4 µm silica colloids with 6 MeV Ag+3 ions irradiation to a fluence of $6.0x10^{14}$ ions/cm^2.

3.2 (I) Au NPs fabricated by using the unmodified mask of 700 nm diameter

In fact, for an ensemble which consists of a distribution of NPs size and shape it is difficult to obtain a detailed correspondence between the NP size and its optical response since only average information is obtained. However, this problem can be overcome by studying single particles in optical microscope, viz., visualization of individual metal NPs in the dark-field optical microscope. Alternatively, the results can be obtained by making sure that all nanoparticles are equal. In the present investigations both possibilities are simultaneously pursued. Figures 7(a-b) show 50x objective images for a sample containing single Au NPs domains with 80-100 nm diameter as viewed under the Nikon dark-field microscope before and after irradiation with 50 MeV Ag^{+7} ions to a fluence of $1.3x10^{15}$ ions/cm^2, (a) and (b), respectively. The hexagonal pattern of the Au NPs is clearly visible. In figure 7(a) one can see that the color for the Au NPs within the hexagonal order is orange. This indicates that the size of the fabricated NPs is relatively large so that their plasmon resonance at approximately 650 nm. These periodic NPs arrays comprise approximately 80% of the total number of fabricated particles. 20% of the recorded particles are fabricated with complex shape as result of dislocation and/or single vacancies in the colloidal mask and therefore cannot be characterized. Some particles appear bright reddish and bright yellowish due to their complex shape in combination with over-exposure by light. In the following we will only consider the effects on the supposingly spherical Au NPs arrays. Figure 7(b) reveals that no color change occurs within the arrays of the Au NPs of 80-100 nm diameter as a result of irradiation with 50 MeV Ag^{+7} ions to a fluence of $1.3x10^{15}$ ions/cm^2. Apparently the Au NPs are not deformed significantly during the swift heavy irradiation, presumably because the stopping power at this stage is not sufficient to induce NP deformation.

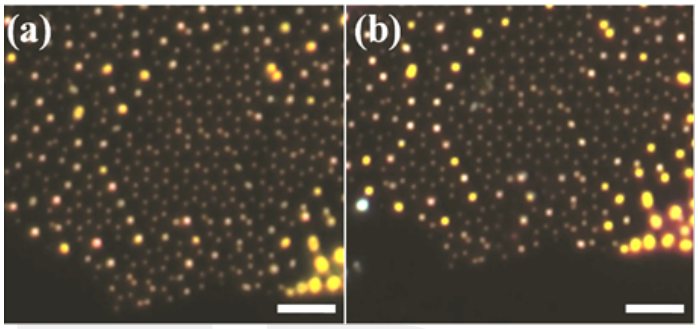

Figure 7 Dark-field light-scattering images of arrays of Au NPs fabricated with 80-100 nm diameter before and after irradiation with 50 MeV Ag^{+7} ions to fluence $1.3x10^{15}$ ions/cm^2, (a) and (b), respectively. The images are taken by the 50x objective and re-scaled with suitable magnification. The scale bar is 0.5 µm.

3.2 (II) Au NPs fabricated by modification of the 1.4 µm silica mask with 6 MeV Ag^{+3} ions to a fluence of $6.0x10^{14}$ ions/cm^2

Figure 8(a) shows a color image of the scattering pattern for a sample containing periodic arrays of Au NPs fabricated with diameter in the range of 50-80 nm before irradiation. The color population in this figure is approximately: 80% of the ordered NPs are green indicating that their surface plasmon resonance is between 500-550 nm, 15-20% of the NPs have a different color, probably because they have a complex shape. The difference in intensity of the Au NPs is due to the different shapes and sizes of the Au NPs present in the hexagonal pattern. After irradiation with 50 MeV Ag^{+7} ions to a fluence of $1.5x10^{15}$ ions/cm^2, the periodic NP arrays shown in figure 8(a) are imaged once again to optically verify the effect

of the Ag swift heavy ion irradiation. The recorded image is shown in figure 8(b). From inspection of the figure, it can be inferred that: (i) 75% of the Au NPs exhibit a red-shift in color, corresponding to the longitudinal plasmon resonance, (ii) 15% of the Au NPs remain green and (iii) 10% of the Au particles are having a complex shape and cannot be characterized and therefore will receive no attention in the discussion of our results.

High resolution transmission electron microscopy (X-TEM) micrographs of Au NPs taken from regions of the sample of figure 8(b) after irradiation with 50 MeV Ag^{+7} ions to a fluence of $1.5x10^{15}$ ions/cm^2, are shown in figures 9(a-b). From inspection of these figures, we distinguish the existence of three populations of NPs: (1) NPs with size presumably larger than 80 nm conserve their spherical shape after SHI irradiation. We identify those NPs as type-1. (2) Elongated NPs with their long axis parallel to the beam direction (type-2), and partially elongated NPs with their long axis along the ion beam direction (type-3).

Within a certain extend, the NPs shape transformation under SHI represents a general behavior of the irradiated NPs, where the key parameter is the size rather than the stopping power, i.e., the larger the NP, the larger its inertia against ion deformation. Therefore, we propose two hypotheses for explanation of presence of type-1 NPs observed within our TEM micrographs. The first hypothesis maybe due to their larger size; presumably NPs are fabricated with diameter > 80 nm where the deformation is almost completely suppressed. Second, alternatively, these NPs maybe fabricated with complex shape as result of dislocation and/or single vacancies in the colloidal mask as shown by the SEM image for few NPs in figure 6. Detailed investigation carried out by authors have led to identify the so-called NP size-dependent energy threshold for elongation [29]. For the applied ion beam of the current study (50 MeV Ag^{+7} ions), the corresponding electronic stopping power deposited by the energetic silver ions is about 7.9 keV.nm^{-1} in the SiO_2 layer and 22.5 keV.nm^{-1} in the Au particles 40). For such applied ion energy, detailed investigations of the role played by NP size within the elongation characteristics (also supported by thermal spike calculations of the temperature elevation around the NP), readily indicate NP size-dependent energy threshold for elongation between 80-100 nm diameter.

As for Au NPs of types 2 and 3 observed within our TEM micrograph in figure 9(a-b), we infer that under irradiation with 50 MeV Ag^{+7} ions to a fluence of $1.5x10^{15}$ ions/cm^2, some of the 50-80 nm Au particles went anisotropic deformation into nanorods, with their long axis parallel to the ion beam direction. These particles appear reddish in the scattering patterns of the Au NPs. In literature, modification of the shape of spherical NPs is known to introduce a variation of the localized surface plasmon resonance; viz the colour of the particles is accordingly changed [23], [24], [25], [30], [31], [32]. On the other hand, the irradiation process follows random statistics and only few of the ion tracks touch the particles. In this sense, the distribution of the energy deposited into the Au NPs as well as the deformation kinetics can be different from one particle to another. In this context, partially deformed NPs can be formed eventhough it should be kept in mind that the ion impact per all NPs is the same; irradiation fluence of $1.5x10^{15}$ ions/cm^2 corresponds on average to 150 ion impacts per each NP.

Kuwata et al. [45] studied the light scattering spectra from individual Au NPs of different morphologies including nanorods, distributed sparsely on a glass cover slide. In this study, for Au nanorods, it is observed that the light is scattered most strongly when the incident polarization is parallel to the long axis, and that the scattering pattern is red-shifted. The latter has been demonstrated in our results for single Au nanorods. Furthermore, we were able to reproduce qualitatively well the typical NPs characteristics in different regions of the sample. This is clear if we consider the same hexagonal close-packed arrays for Au NPs before and after irradiation with 50 MeV Ag^{+7} ions to a fluence of $1.5x10^{15}$ ions/cm^2, figure 10(a) and figure 10(b), respectively. The color population in figures 10(a) reveals approximately 75% of the particles within the hexagonal order are green and ~ 20% of the particles have a different color and/or complex shape. After 50 MeV Ag^{+7} ion irradiation to fluence $1.5x10^{15}$ ions/cm^2, the color population in figures 10(b) reveals ~ 60-70% of the greenish particles are turned into red particles while 15% are still green. The incident white light strikes the samples under ~45 degrees with respect to the sample surface. From these observations, it appears clearly that the shaping effects, induced by silver swift heavy ions on the hexagonal arrays of Au NPs have decisive influence on their optical response.

To conclude, in this subsection we have optically distinguished the color characteristics of hexagonal close-packed arrays of Au NPs fabricated by NSL by imaging their scattering patterns in a dark-field optical microscope. Our experimental findings are that no difference in color is observed within the scattering patterns of Au NPs with diameter of 80-100 nm before and after irradiation with 50 MeV Ag^{+7} ions to a fluence of $1.5x10^{15}$ ions/cm^2. This suggests that the elongation of such NPs does not measurably occur under irradiation with

this energy. However, it is concluded that the irradiation induced color change from green to red at many of the ordered arrays of Au NPs of 50-80 nm is a result of their elongation as they are traversed by the silver swift heavy ions irradiation.

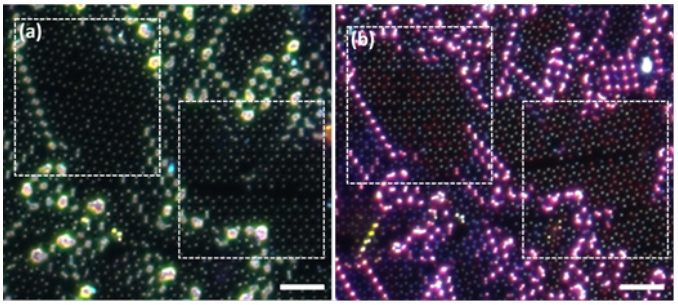

Fig. 8 Dark-field light-scattering images for different areas of a sample containing Au NPs of ~50-80 nm diameter before and after irradiation with 50 MeV Ag^{+7} ions to the maximum fluence of $1.5x10^{15}$ ions/cm^2, a and b, respectively. After irradiation, most of the greenish colored particles have become reddish colored due to the ion-shaping effect. Images are re-scaled with suitable magnification. The scale bar is 0.5 μm.

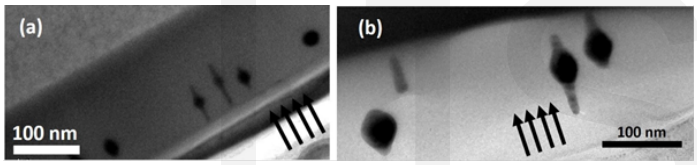

Fig. 9 X-TEM images of Au NPs with average size between 50-100 nm fabricated by NSL after being irradiated with 50 MeV Ag^{+7} ions to a fluence of $1.5x10^{15}$ ions/cm^2, (a) and (b), respectively. Black arrows indicate the ion beam direction. Scale bar in images (a) and (b) is 100 nm.

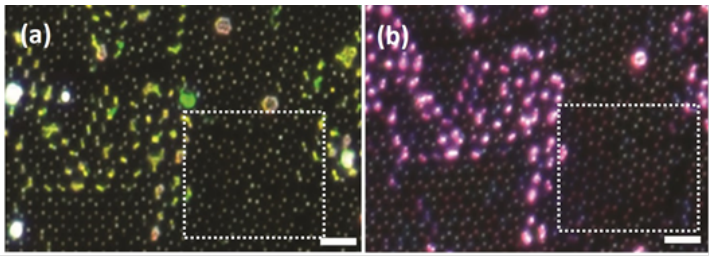

Fig.10 Dark-field light-scattering images for different areas of a sample containing Au NPs of ~50-80 nm diameter before and after irradiation with 50 MeV Ag^{+7} ions to the maximum fluence of $1.5x10^{15}$ ions/cm^2, (a) and (b), respectively. After irradiation, most of the greenish colored particles have become reddish colored due to the ion-shaping effect. Images are rescaled with suitable magnification. The scale bar is 0.5 μm.

4 Conclusions

In conclusions, we have shown to be able to fabricate ordered arrays of Au NPs with diameter in the range between 50-100 nm by using two variants of self-assembled colloidal crystal deposition masks. In addition, we were able to modify the size and shape of the fabricated Au NPs by adjustment of the deposition mask and alternatively, by optimization of the different irradiation parameters. Furthermore, we have optically distinguished the color characteristics of hexagonal close-packed arrays of Au NPs fabricated by NSL by imaging their scattering patterns in a dark-field optical microscope. Our experimental findings are that no difference in color is observed within the scattering patterns of Au NPs with diameter of 80-100 nm before and after irradiation with 50 MeV Ag^{+7} ions to a fluence of $1.5x10^{15}$ ions/cm^2. This suggests that the elongation of such NPs does not measurably occur under irradiation with this energy. However, it is concluded that the irradiation induced color change from green to red at many of the ordered arrays of Au NPs of 50-80 nm is a result of their elongation as they are traversed by the silver swift heavy ions irradiation.

References

[1] Van Blaaderen, R. Ruel, and P. Wiltzius, "Template-directed colloidal crystallization," Nature 385, 321-324 (1997).

[2] Y. Yin, Y. Lu, B. Gates, and Y. Xia, "Template-Assisted Self-Assembly: A Practical Route to Complex Aggregates of Monodispersed Colloids with Well-Defined Sizes, Shapes, and Structures," J. Am. Chem. Soc. 123 (36), 8718–8729 (2001).

[3] D. Xia and S. R. J. Brueck, "A Facile Approach to Directed Assembly of Patterns of Nanoparticles Using Interference Lithography and Spin Coating," Nano Lett. 4 (7), 1295–1299 (2004).

[4] S. Liu, R. Maoz and J. Sagiv, "Planned Nanostructures of Colloidal Gold via Self-Assembly on Hierarchically Assembled Organic Bilayer Template Patterns with In-situ Generated Terminal Amino Functionality," Nano Lett. 4(5), 845–851 (2004).

[5] J.C. Hulteen and R.P. Van Duyne, "Nanosphere lithography: A materials general fabrication process for periodic particle array surfaces," J. Vac. Sci.

technol. A (13), No. 3, 1553-1558 (1995).
[6] S. Aştilean, "Fabrication of periodic metallic nanostructures by using nanosphere lithography," Romanian Reports in Physics, Volume 56, No. 3, 340-345 (2004).
[7] Pierre Colson, Catherine Henrist and Rudi Cloots, "Nanosphere Lithography: A Powerful Method for the Controlled Manufacturing of Nanomaterials, "Journal of Nanomaterials, Volume 2013, 948510-948528 (2013).
[8] P. Pieranski, "Two-Dimensional Interfacial Colloidal Crystals," Physical Review Letters, vol. 45, no. 7, 569-572 (1980).
[9] G. Zhang and D. Wang, "Colloidal Lithography-The Art of Nanochemical Patterning," Chemistry, vol. 4, no. 2, 236-245 (2009).
[10] S.-M. Yang, S. G. Jang, D.-G. Choi, S. Kim, and H. K. Yu, "Nanomachining by colloidal lithography," Small, vol. 2, no. 4, 4584-75, (2006).
[11] U. Fischer and H. P. Zingsheim, "Submicroscopic pattern replication with visible light, "J. Vac. Sci. Technol. 19, (4), 881-885, (1981).
[12] H. W. Deckman and J. H. Dunsmuir, "Natural lithography," Applied Physics Letters, vol. 41, no. 4, 377-379, (1982).
[13] H. W. Deckman and J. H. Dunsmuir, "Applications of surface texture produced with natural lithography," Journal of Vacuum Science and Technology B, vol. 1, no. 4, 1109–1112, (1983).
[14] S. Connolly and D. Fitzmaurice, "Programmed Assembly of Gold Nanocrystals in Aqueous Solution," Adv. Mater. 11, 1202-1205 (1999).
[15] Ming Zheng and Xueying Huang, "Biofunctionalization of Nanomaterials," Nanotechnologies for the Life Sciences Vol. 1, 1-353, (2005).
[16] M. Winzer, M. Kleiber, N. Dix and R. Wiesendanger, "Fabrication of nano-dot- and nano-ring-arrays by nanosphere lithography," Appl. Phys. A. 63, 617-619 (1996).
[17] C. L. Haynes and R. P. Van Duyne, "Nanosphere Lithography: A Versatile Nanofabrication Tool for Studies of Size-Dependent Nanoparticle Optics," J. Phys. Chem. B 105 (24) 5599-5611, (2001).
[18] X. Huang, D. Ratchford, P. E. Pehrsson and J. Yeom, "Fabrication of metallic nanodisc hexagonal arrays using nanosphere lithography and two-step lift-off," Nanotechnology, 27, 395302- 395312, (2016).
[19] John C. Hulteen, David A. Treichel, Matthew T. Smith, Michelle L. Duval, Traci R. Jensen, and Richard P. Van Duyne, "Nanosphere Lithography: Size-Tunable Silver Nanoparticle and Surface Cluster Arrays," J. Phys. Chem. B, 103,(19), 3854-3863 (1999).
[20] C. X. Cong, T. Yu, Z. H. Ni, L. Liu, Z. X. Shen, and W. Huang, "Fabrication of Graphene Nanodisk Arrays Using Nanosphere Lithography, " J. Phys. Chem. C, 113 (16), 6529-6532, (2009).
[21] Traci R. Jensen, Michelle Duval Malinsky, Christy L. Haynes, and Richard P. Van Duyne, J. Phys. Chem. B,45 (104), 10549-10556, (2000).
[22] Teun van Dillen, Alfons van Blaaderen, Albert Polman, "Shaping colloidal assemblies," material today review, Volume 7, Issues 7–8, 40-46, (2004).
[23] T. van Dillen and A. Polman, W. Fukarek, A. van Blaaderen, "Energy-dependent anisotropic deformation of colloidal silica particles under MeV Au irradiation," Appl. Phys. Lett. 78, (7) 910-912, (2001).
[24] J.J.Penninkhof, T.van Dillen, S.Roorda, C.Graf, A.van Blaaderen, A.M.Vredenberg and A.Polman, "Anisotropic deformation of metallo-dielectric core–shell colloids under MeV ion irradiation," NIMB, Volume 242, Issues 1–2, 523-529, (2006).
[25] T. van Dillen, "Ion irradiation-induced anisotropic plastic deformation," Ph.D. thesis, ISBN: 9039336709, (2004).
[26] D. L. J. Vossen, D. Fific, J. Penninkhof, T. van Dillen, A. Polman and A. van Blaaderen, "Combined Optical Tweezers/Ion Beam Technique to Tune Colloidal Masks for Nanolithography," Nano Lett. Vol. 5, No. 6, 1175–1179, (2005).
[27] J. Penninkhof, "Tunable plasmon resonances in anisotropic metal nanostructures," Ph.D. thesis, ISBN: 978-90-393-4316-6 (2006).
[28] Roorda, T. van Dillen, A. Polman, C. Graf, A. M. Vredenberg, A. van Blaaderen, and B. Kooi, " Aligned Gold Nanorods in Silica Made by Ion Irradiation of Core–Shell Colloidal Particles," Adv. Mater. (Weinheim, Ger.) 16, 235-237 (2004).
[29] J. J. Penninkhof, T. van Dillen, A. Polman, C. Graf, and A. van Blaaderen, "Angle-Dependent Extinction of Anisotropic Silica/Au Core/Shell Colloids Made via Ion Irradiation," Adv. Mater. (Weinheim, Ger.) 17, 1484-1488 (2005).
[30] J. J. Penninkhof, T. van Dillen, S. Roorda, C.Graf, A. vanBlaaderen, A. M. Vredenberg, and A. Polman, "Anisotropic deformation of metallo-dielectric core-shell colloids under MeV ion irradiation," Nucl. Instr.Methods Phys. Res., Sect. B 242, 523-529 (2006).
[31] E. A. Dawi, G. Rizza, M. P. Mink, A. M. Vredenberg, and F. H. P. M. Habraken, "Ion beam shaping of Au nanoparticles in silica: Particle size and concentration dependence,"J. Appl. Phys. 105, 074305-074313 (2009).
[32] G. Rizza, E. A. Dawi, A. M. Vredenberg, and I. Monnet, "Ion engineering of embedded nanostructures: From spherical to facetted nanoparticles," Appl. Phys. Lett. 95, 043105- 043107 (2009).
[33] E. A. Dawi, A. M. Vredenberg, G. Rizza, and M. Toulemeonde, "Ion-induced elongation of gold nanoparticles in silica by irradiation with Ag and Cu swift heavy ions: track radius and energy loss threshold," Nanotechnology 22, 215607-21619, (2011).
[34] G. Rizza, F. Attouchi, P.-E. Coulon, S. Perruchas, T. Gacoin, I. Monnet, and L. Largeau," Rayleigh-like instability in the ion-shaping of Au–Ag alloy nanoparticles embedded within a silica matrix," Nanotechnology 22, 175305 (2001).
[35] K. Awazu, X. Wang, M. Fujimaki, J. Tominaga, H. Aiba, Y. Ohki, and T. Komatsubara, "Elongation of gold nanoparticles in silica glass by irradiation with swift heavy ions," Phys. Rev. B 78, 054102-054109 (2008).
[36] R. Giulian, P. Kluth, L. L. Araujo, D. J. Sprouster, A. P. Byrne, D. J. Cookson, and M. C. Ridgway, "Shape transformation of Pt nanoparticles induced by swift heavy-ion irradiation," Phys. Rev. B 78, 125413-125420 (2008).
[37] M. C. Ridgway, P. Kluth, R. Giulian, D. Sprouster, L. L. Araujo, C. Schnohr, D. Llewellyn, A. Byrne, G. Foran, and D. Cookson, "Changes in metal nanoparticle shape and size induced by swift heavy-ion irradiation," Nucl. Instrum. Methods Phys. Res., Sect. B 267, 931-935 (2009).
[38] D. Sprouster, R. Giulian, L. L. Araujo, P. Kluth, B. Johannessen,D. Cookson, and M.C.Ridgway, "Swift heavy-ion irradiation-induced shape and structural transformation in cobalt nanoparticles," J. Appl. Phys. 109, 113504-113510 (2011).

[39] M. C. Ridgway, R. Giulian, D. J. Sprouster, P. Kluth, L. L. Araujo, D. J. Llewellyn, A. P. Byrne, F. Kremer, P. F. P. Fichtner, G. Rizza, H. Amekura, and M. Toulemonde, "Role of Thermodynamics in the Shape Transformation of Embedded Metal Nanoparticles Induced by Swift Heavy-Ion Irradiation," Phys. Rev. Lett. 106, 095505-095508 (2011).
[40] G. Rizza, P. E. Coulon, V. Khomenkov, C. Dufour, I. Monnet, and M. Toulemonde, S. Perruchas, T. Gacoin, D. Mailly, X. Lafosse, C. Ulysse and E. A. Dawi, "Rational description of the ion-beam shaping mechanism," PRB 86, 035450- 035457 (2012).
[41] C. Dufour, V. Khomenkov, G. Rizza, and M. Toulemonde, "Ion-matter interaction: the three-dimensional version of the thermal spike model. Application to nanoparticle irradiation with swift heavy ions," J. Phys. D, 45, 065302 (2012).
[42] S. Klaumünzer, Nucl. Instr. and Meth. in Phys. Res. B 244, (2006) 1.
[43] K. Awazu, X. Wang, M. Fijimaki and J. Tominga, "Elongation of gold nanoparticles in silica glass by irradiation with swift heavy ions, "Phys. Rev. B 78 054102-054109 (2008).
[44] J. F. Ziegler, J. P.Biersack and M. D. Ziegler, SRIM–A version of the TRIM program, The Stopping and Range of Ions in Matter (2008), (http://www.srim.org).
[45] H. Kuwata, H. Tamaru, K. Esumi, and K. Miyano, "Resonant light scattering from metal nanoparticles: Practical analysis beyond Rayleigh approximation," Appl. Phys. Lett. 83, 4625-4627, (2003).